Optimization-based calibration of hydrodynamic drag coefficients for a semisubmersible platform using experimental data of an irregular sea state

M Böhm[1], A Robertson[2], C Hübler[3], R Rolfes[3] and P Schaumann[1]

[1] Institute for Steel Construction, Leibniz University Hannover - ForWind, Appelstrasse 9, 30167 Hannover, Germany
[2] National Renewable Energy Laboratory, Golden, Colorado, USA
[3] Institute of Structural Analysis, Leibniz University Hannover - ForWind, Appelstrasse 9, 30167 Hannover, Germany

E-mail: boehm@stahl.uni-hannover.de

Abstract. For the simulation of the coupled dynamic response of floating offshore wind turbines, it is crucial to calibrate the hydrodynamic damping with experimental data. The aim of this work is to find a set of hydrodynamic drag coefficients for the semisubmersible platform of the Offshore Code Comparison Collaboration, Continuation, with Correlation and unCertainity (OC6) project which provides suitable results for an irregular sea state. Due to the complex interaction of several degrees of freedom (DOF), it is common to calibrate drag coefficients with the time series of decay tests. However, applying these drag coefficients for the simulation of an irregular sea state results in misprediction of the motions. By using numerical optimization, it is possible to calibrate multiple drag coefficients simultaneously and effectively, while also considering several DOF. This work considers time series of structural displacements from wave tank tests of the OC6 project and from simulations of the same load cases in OpenFAST. Results are transferred into the frequency domain and the deviation between power spectral densities of surge, pitch and heave from experiment and numerical simulation is used as an objective function to obtain the best fitting drag coefficients. This novel numerical optimization approach enables finding one set of drag coefficients for different load cases, which is a major improvement compared to decay-test-tuned drag coefficients.

1. Introduction

With increasing demand for renewable energies, further development and improvement of the technologies is necessary. Wind energy is now the second largest renewable energy sector after hydropower [1], and has the potential to be first in the near future. Offshore, there are vast wind resources, of which 60% to 80% are located in sites with water depths of 60 m and more [2, 3]. At these sites, the wind is stronger and more consistent, allowing a higher and more reliable power production than onshore. Economically feasible designs for deep-water sites are expected to require floating substructures. In order to enable further development and optimization of the floating structures, it is necessary to predict structural loads accurately, which depend on system damping.

Within the Offshore Code Comparison Collaboration, Continued, with Correlation (OC5) project, simulation results of a floating wind semisubmersible were validated against

measurements from a scaled test campaign performed at the Maritime Research Institute Netherlands [4]. Although the coupled engineering level tools captured many dynamic interactions of the floater, a persistent underprediction of the motions in the low-frequency region was observed [4]. The largest differences were found below the primary wave frequency range and associated with the pitch and surge natural frequencies. This low-frequency excitation is created by nonlinearities of the wave forces, through interaction of different wave components. It is assumed that a combination of underpredicting the nonlinear loading and overpredicting (or misrepresenting) the damping in the system is the cause for the underprediction of motions. The follow-up OC6 project focuses on the validation of the nonlinear hydrodynamic effects in phase I, neglecting the aerodynamic interaction.

To calculate hydrodynamic forces, it is common to use engineering-level tools with a hybrid formulation: Diffraction and radiation forces from a potential flow model and additional viscous drag, computed with the drag-term from Morison's equation, are superimposed. Drag forces and the hydrodynamic quadratic damping directly depend on the choice of the viscous drag coefficients. In wind energy engineering, these drag coefficients are usually calibrated to match experimental results. Due to reasons of feasibility, it is a common approach to derive the drag coefficients from decay tests [5]. Recent studies [6, 7, 8] revealed that identifying load-case-specific drag coefficients leads to significantly better agreement of the low-frequency platform response between the simulation and experiment. However, manual parameter fitting allows one to only consider a limited number of drag coefficient combinations. To calibrate drag coefficients effectively, a more advanced method is needed. In this work, drag coefficients are tuned to match the response of the semisubmersible in decay tests as well as in an irregular sea state, where the latter case is calibrated using numerical optimization instead of manual parameter fitting.

The outline of the paper is as follows. First, an overview of the modelling assumptions is provided and then, drag coefficient tuning using decay test measurements is described. The next section focuses on the calibration with numerical optimization. Finally, a comparison of decay-test-tuned drag coefficients and irregular wave-tuned coefficients is presented, conclusions are drawn and considerations for future work are summarized.

2. Model

For this work, data from the first test campaign of the OC6 project phase I [9] is considered. The floating wind turbine model is similar to the OC5-DeepCwind semisubmersible [4], consisting of three offset columns with heave plates connected through pontoons and braces to a central column, as shown in Figure 1. All components are cylindrical. The structure is moored via three taut spring lines attached to the offset columns. To focus on hydrodynamic impacts only, the model has no nacelle, rotor or blades; mass and inertia properties of the tower and rotor nacelle assembly are largely maintained by employing a rigid tower.

The modularized floating wind simulation tool, OpenFAST [10], developed by the National Renewable Energy Laboratory, is used to simulate the coupled dynamic response of all components of the wind turbine power plant. To match the natural frequencies, a modal tuning of the numerical model is performed using the decay test results. Structural properties are adjusted within the boundaries of systematic uncertainty according to Robertson et al. [11]. All properties of the numerical model are scaled up from the 1/50 scale physical experiment, considering a constant Froude number. The most relevant platform and mooring line properties are given in Table 1 considering the results from modal tuning.

For the hydrodynamic model, a hybrid formulation including second-order potential flow and drag terms from the relative form of Morison equation is applied. The wave diffraction and radiation from potential flow theory is calculated with the panel code WAMIT and then used as input for the OpenFAST simulations. For this calibration, the WAMIT files from the OC4 reference model are considered. Besides the hydrodynamics (calculated by the module

Table 1. Full-scale model parameters after modal calibration

Platform and mooring line properties		Geometry of the platform	
Platform mass	4 196 250 kg	Total draft	20 m
Center of mass from SWL [a]	−7.32 m	Length main column	30 m
I_{yy} about COG [b]	$12\,979 \times 10^6$ kg^2 m	Diameter main column	6.5 m
Mooring line length	55.432 m	Length offset columns	26 m
Mooring line diameter	0.004 m	Diameter offset columns	12 m
EA mooring lines	2 908 000 N	Length of heave plates	6 m
Displaced volume	14 039.8 m^3	Diameter of heave plates	24 m

[a] Sea water level, [b] Center of gravity

HydroDyn), the elastodynamic behaviour (using the module ElastoDyn) and the mooring line behaviour (using MAP++) are considered.

3. Calibration of hydrodynamic drag coefficients

In this section, the calibration of the linear and quadratic damping with decay tests in calm water is described. Further, a novel numerical optimization approach to calibrate drag coefficients with irregular waves is introduced. Whereas most linear damping originates from radiation, the largest proportion of quadratic damping is due to viscous drag. Hence, the terms quadratic damping and drag are used interchangeably, while the term damping without additions refers to linear as well as quadratic contributions. The quadratic damping due to drag is numerically specified by coefficients C_D, which are adjusted to fit experimental data. This procedure is described in the following subsections.

3.1. Calibration of damping using decay tests

To calibrate the damping with decay tests, linear and quadratic damping measured in the physical experiment are identified by plotting the damping ratio as a function of the mean amplitude (p-q-method) [12]. To adjust the damping terms, the experimental results are compared to numerical free-decay tests, starting without any drag terms or additional linear damping, considering only the linear damping from radiation. The decay in the heave, surge and pitch directions (coordinate system shown in Figure 2), is calibrated successively in the mentioned order by increasing the drag terms first and then adding linear damping with the additional linear damping matrix if necessary. For the tuning, seven oscillation periods are considered.

In the numerical simulation, transverse C_D and axial drag coefficients, C_{Dz}, are considered. Taking into account the impact of different cylinder dimensions, as shown in Figure 1, two drag coefficient distributions are considered: The first distribution includes a transverse drag coefficient for heave plates, C_{Dh}, a transverse drag coefficient for all other structural members, C_{Do}, and an axial drag coefficient, C_{Dz}, for the heave plates, shown in Figure 1. C_{Dz} is a doubled value, which is only applied on the bottom of the heave plate and not on the top. This calibration leads to the following drag coefficients: 8.2 for C_{Dz}, 1.6 for C_{Dh} and 0.4 for C_{Do}. The second setting considers a uniform transverse drag coefficient $C_{Dh} = C_{Do}$ and an axial drag coefficient for the heave plates, resulting in 0.8 for C_D and 8.2 for C_{Dz}. The drag coefficients are summarized and compared to the other results in Figure 10.

Both drag coefficient distributions result in equally good agreement between experimental and numerical decay. Therefore, this method of calibration is not suited to derive the distribution of drag coefficients between upper columns, other members and heave plates. The agreement

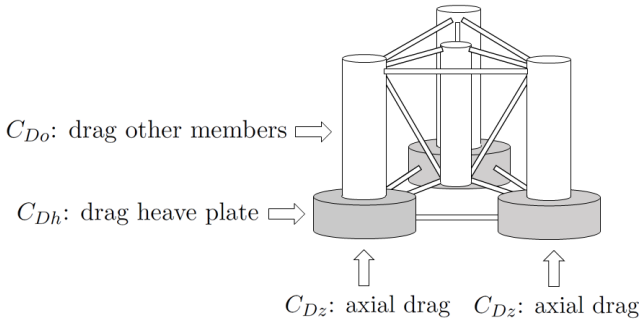

Figure 1. Distribution of the drag coefficient when two transverse coefficients are applied

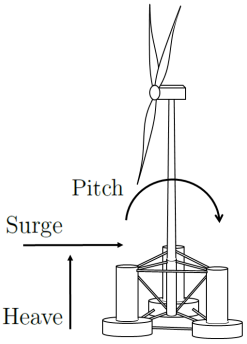

Figure 2. semisubmersible with turbine and directions

between the experiment and calibrated model with a distributed transverse drag coefficient is shown in Figure 3. For pitch and surge, it is necessary to add a term into the additional linear damping matrix to match the linear damping characteristics of the model during small-amplitude free-decay oscillations. The added linear damping coefficients result in $75 \times 10^3\,\mathrm{N\,s\,m^{-1}}$ for surge and $31 \times 10^6\,\mathrm{N\,m\,s\,rad^{-1}}$ for pitch.

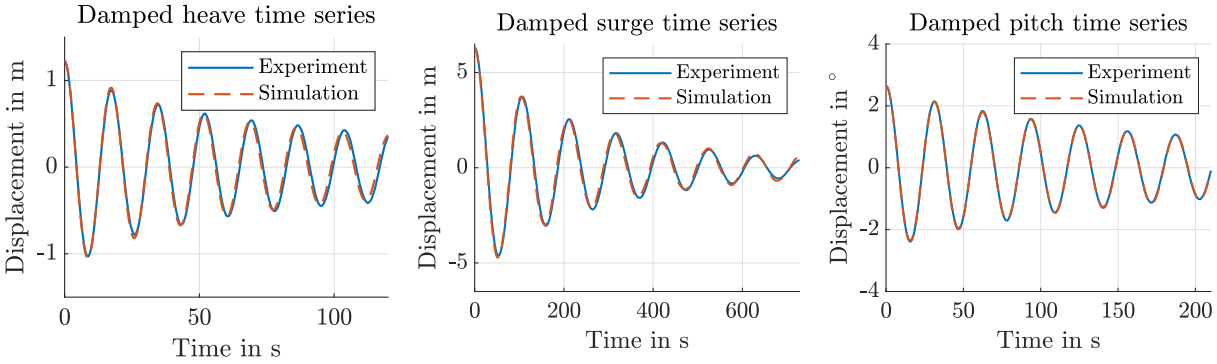

Figure 3. Time series of the experiment and simulation for calibrated heave, surge and pitch decay considering three drag coefficients

3.2. Numerical optimization scheme

A simulation of the irregular sea state from the test campaign with a JONSWAP spectrum, a significant wave height of 7.1 m, a peak period of 12.1 s and $\gamma = 3.3$ shows that the drag coefficients obtained by the calibration using the decay tests do not lead to good results for simulations with waves. As shown in Figure 4, the heave motion in the simulation matches the measured motion, but the surge and pitch motion are not well represented. The responses are generally too small, which may be caused by too much damping. This indicates that a separate calibration of the damping for this load case is reasonable. To consider various drag coefficient distributions, a global numerical optimization algorithm is used to find the best-fitting coefficients.

At first, the measured irregular wave data is processed to be in a suitable format for a numerical optimization. The signal is shortened into two segments of 3660 seconds, one is used for calibration and one is used for validation. The wave elevation is used as input for the OpenFAST simulations. The first 60 seconds are eliminated to remove start-up transients, as

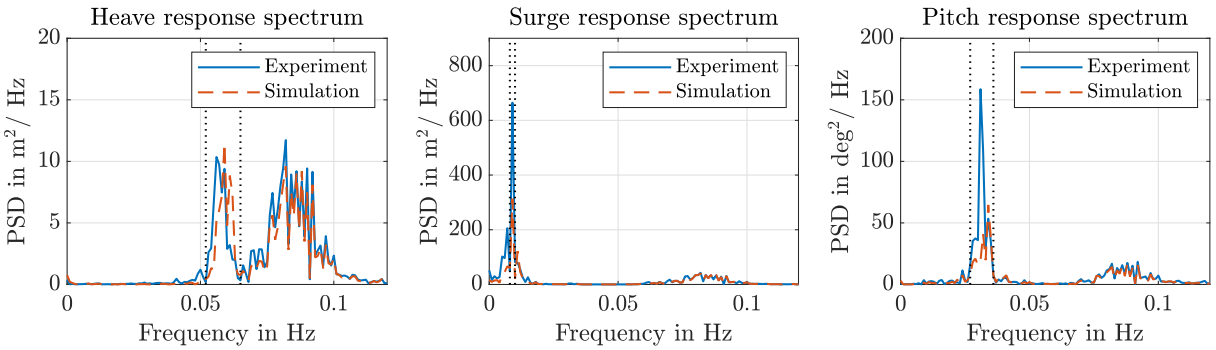

Figure 4. Power spectral densities (PSDs) of the experiment and simulation; relevant frequency bands for the numerical optimization are indicated by dotted lines

recommended by Haid [13], leaving 1 hour of irregular sea state data available for the evaluation. Numerical and experimental displacement time series are transferred into the frequency domain by applying a fast Fourier transform to obtain one-sided power spectral densities (PSDs). The spectra are smoothened with Bartlett's method, yielding a resolution of 0.001 Hz to capture the extremely low natural frequencies.

For the numerical optimization within this work, the global pattern search algorithm [14] was utilized. Comparison with a genetic algorithm [15] in a test run of this problem proved it to be much more efficient. The global pattern search is set to track 10 minima. Further, C_{Dh}, C_{Do} and C_{Dz} are selected as the design variables and updated in every iteration

$$\boldsymbol{x} = \begin{bmatrix} C_{Dh} & C_{Do} & C_{Dz} \end{bmatrix}^{\mathrm{T}}. \tag{1}$$

The parameter space of the design variables is limited to lower and upper bounds

$$\begin{bmatrix} 0.1 & 0.1 & 3.0 \end{bmatrix}^{\mathrm{T}} \leq \boldsymbol{x} \leq \begin{bmatrix} 3.0 & 3.0 & 10.0 \end{bmatrix}^{\mathrm{T}}. \tag{2}$$

Additionally, an objective function $\varepsilon(\boldsymbol{x})$ is formulated for each drag coefficient distribution. This function constitutes the difference between experimental and numerical responses and is numerically minimized. Thus, values close to zero indicate good agreement between the simulation and experiment. There are several requirements for the objective function: Motion responses in heave, surge and pitch direction should be considered. It has to be sensitive to small changes of the peak frequencies, whereas differing noise levels should not affect the comparison. As the choice of the drag coefficients does not have a significant impact on the response to first-order forces in the range between 0.06 and 0.11 Hz, only the low-frequency region can be considered. After considering and testing several options for the formulation of the objective function, an evaluation of the band power in relevant frequency bands is selected. By suitably choosing bandwidth, the above mentioned requirements are fulfilled. The average band power $\mathrm{P}_{\mathrm{band}}$ over a certain frequency band from the lower discrete frequency l to the upper discrete frequency u is calculated by

$$\mathrm{P}_{\mathrm{band}} = \frac{\sum_{i=l}^{u} \mathrm{PSD}(f_i)}{u - l + 1}, \tag{3}$$

where f_i are the discrete frequencies obtained from the fast Fourier transform. As measurement of the fit, the ratio between the measured average power in the relevant band and the simulated average power in the relevant band is determined. The relevant frequency band of pitch ranges from 0.027 Hz to 0.036 Hz, whereas for surge the boundaries are 0.008 Hz and 0.010 Hz. A wider

band has to be used for heave, due to the slight frequency shift. The limits of this band are 0.052 Hz and 0.065 Hz. All frequency bands are marked in Figure 4 with dashed lines.

Since a high contribution of linear damping has been observed in the decay tests, it is assumed that this damping is external (i.e. stemming from the experimental apparatus). For this reason, the value from the decay test calibration is maintained for the simulation of the irregular wave test.

3.3. Single-objective optimization

Initially, the objective is to find one optimal solution for all three degrees of freedom. Thus, three drag coefficients, one axial and two transverse, are optimized. After conducting a prestudy, the bounds of the parameter space are set according to Eq. 2. Further, this prestudy shows that surge motions are only affected by transverse drag coefficients, heave motions are only affected by the axial drag coefficients and pitch motions are mainly affected by the axial drag coefficient. Besides, it became obvious that considering equal weighting of heave and pitch leads to a mismatch of both responses. It is thus not possible to find a good solution for the axial drag coefficient, which affects both heave and pitch. A possible reason is that the pitch damping may not be well represented by the current OpenFAST model. This leads to the decision to weigh the pitch response less for this first optimization approach and to formulate the objective function as follows

$$\varepsilon(\boldsymbol{x}) = \frac{\left|\mathrm{P}^{\mathrm{S,h}}_{\mathrm{band}} - \mathrm{P}^{\mathrm{E,h}}_{\mathrm{band}}\right|}{\mathrm{P}^{\mathrm{E,h}}_{\mathrm{band}}} + \frac{\left|\mathrm{P}^{\mathrm{S,s}}_{\mathrm{band}} - \mathrm{P}^{\mathrm{E,s}}_{\mathrm{band}}\right|}{\mathrm{P}^{\mathrm{E,s}}_{\mathrm{band}}} + 0.5 \cdot \frac{\left|\mathrm{P}^{\mathrm{S,p}}_{\mathrm{band}} - \mathrm{P}^{\mathrm{E,p}}_{\mathrm{band}}\right|}{\mathrm{P}^{\mathrm{E,p}}_{\mathrm{band}}}, \tag{4}$$

where $\mathrm{P}_{\mathrm{band}}$ is calculated using Eq. 3. The index S denotes simulation, E denotes experiment, h heave, s surge and p pitch. The optimized drag coefficients are 7.4 for C_{Dz}, 0.1 for C_{Dh} and 0.84 for C_{Do}. As shown in Figure 5, this compromise results in an underprediction of pitch, but the prediction of the surge motion is significantly improved compared to the decay-test-tuned response.

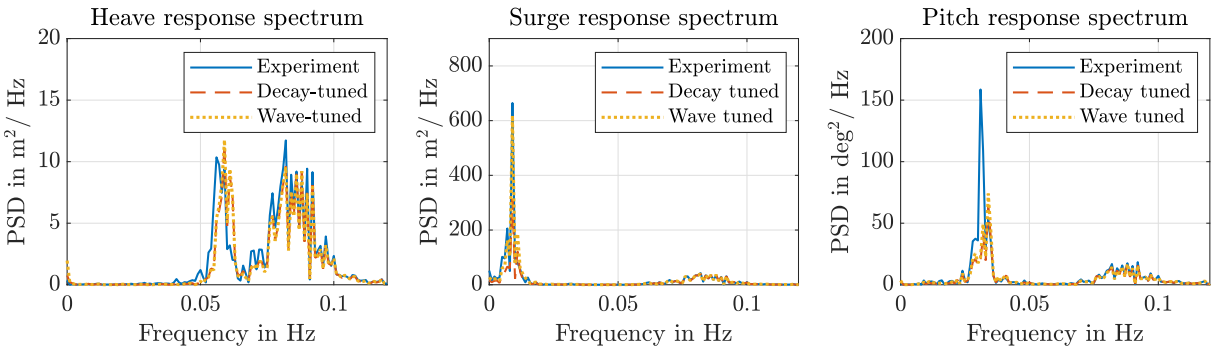

Figure 5. Comparison of PSDs with optimized drag coefficients (calibration results) and decay-test-tuned drag coefficients

To validate the result, another time interval of the measured irregular wave response, containing the same significant wave height, period and shape factor, is utilized. The optimized drag coefficients for the optimization including linear damping, represent the measured motions well. As expected, the only exception is the pitch motion, where the optimization does not yield good results because of the lower weighting. This means that for an irregular wave it is not possible to find an axial drag coefficient that represents heave and pitch damping well.

3.4. Multiobjective optimization for two design variables

The findings of the previous section show that it is not possible to calibrate the drag coefficients in a way that all motion responses in surge, heave and pitch direction are represented well using a single objective function. Thus, a multiobjective optimization is applied using two different objective functions to quantify the discrepancy between optimal solutions for heave and pitch. The first objective function $\varepsilon_1(\boldsymbol{x})$ considers the agreement of heave and surge responses and the second objective function $\varepsilon_2(\boldsymbol{x})$ considers the agreement of the pitch motion

$$\varepsilon_1(\boldsymbol{x}) = \frac{\left|\mathrm{P}^{\mathrm{S,h}}_{\mathrm{band}} - \mathrm{P}^{\mathrm{E,h}}_{\mathrm{band}}\right|}{\mathrm{P}^{\mathrm{E,h}}_{\mathrm{band}}} + \frac{\left|\mathrm{P}^{\mathrm{S,s}}_{\mathrm{band}} - \mathrm{P}^{\mathrm{E,s}}_{\mathrm{band}}\right|}{\mathrm{P}^{\mathrm{E,s}}_{\mathrm{band}}}, \qquad \varepsilon_2(\boldsymbol{x}) = \frac{\left|\mathrm{P}^{\mathrm{S,p}}_{\mathrm{band}} - \mathrm{P}^{\mathrm{E,p}}_{\mathrm{band}}\right|}{\mathrm{P}^{\mathrm{E,p}}_{\mathrm{band}}}. \tag{5}$$

Within this multiobjective optimization, the focus is on the axial drag coefficient and a uniform transverse drag coefficient is considered (i.e., $C_{Dh} = C_{Do}$). According to Eq. 2, the bounds of the parameter space are chosen. For the optimization, the multiobjective global pattern search approach is used.

After 1023 evaluations, a clear Pareto front has developed in the objective value space, as shown in Figure 6. In the design variable space, optimum HS yields the best drag coefficients for heave and surge, since values of ε_1 are minimized, and optimum P yields the best solution for pitch, where ε_2 is diminished. The corresponding values are given by

$$\boldsymbol{x}_{\mathrm{HS}} = \begin{bmatrix}0.37 & 0.37 & 7.6\end{bmatrix}^{\mathrm{T}} \qquad \text{and} \qquad \boldsymbol{x}_{\mathrm{P}} = \begin{bmatrix}0.53 & 0.53 & 3.9\end{bmatrix}^{\mathrm{T}} \tag{6}$$

and are shown in Figure 10.

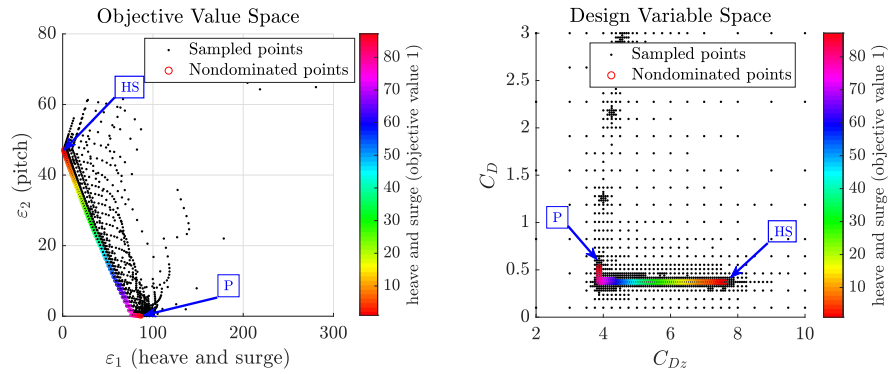

Figure 6. The Pareto front of the multiobjective formulation and the associated sampling points in the design variable space, considering two variables

The response spectra for both ends of the Pareto front are shown in Figure 7. On one side, optimum HS is the optimal solution for heave and surge, showing large discrepancies between the simulation and experiment for pitch. On the other side, optimum P is the optimized solution for pitch, showing a large difference between the simulation and experiment for heave. Optimal solutions for $C_{Dh} = C_{Do}$ are in a similar range, whereas it is not possible to find a compromise for C_{Dz}.

3.5. Multiobjective optimization for three design variables

Further, a multiobjective optimization for all three drag coefficients is performed. The objective functions from Eq. 5 are maintained and the design variable space according to Eq. 2 is adopted. Again, the multiobjective global pattern search is applied. The optimization was terminated

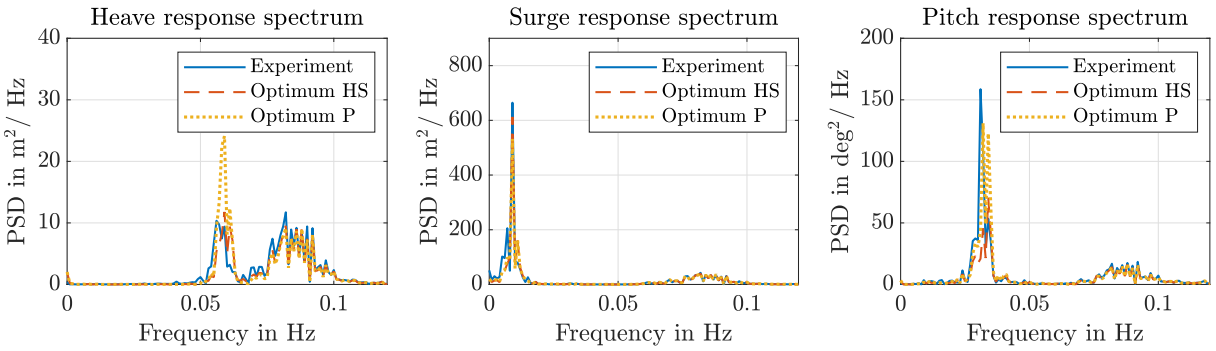

Figure 7. PSDs with optimized drag coefficients for heave, surge (HS) and pitch (P), using two design variables

after 1522 iterations, when the design variable space was evaluated to a resolution of the first decimal. Optimizing for all three coefficients, the Pareto front moves toward lower objective values (i.e., matches better), see Figure 8, compared to a uniform transverse drag coefficient. Considering the design variable space, the optimum for surge and heave is found for 7.5 for C_{Dz}, 0.1 for C_{Dh} and 0.83 for C_{Do}. The magnitude of the values agrees with the optimum for the single objective optimization. For pitch, the optimum is found for the same transverse drag coefficients and for a C_{Dz} of 4.0.

Conspicuous is the fact that the results located in the central part of the Pareto front are found in a different area in the design variable space. Values are around 5.4 for C_{Dz} and 2.9 for C_{Do}. The power spectral densities for optimal solutions for both objective functions are shown in Figure 9. Both solutions on the ends of the Pareto front resemble the results from the multiobjective optimization with two design variables.

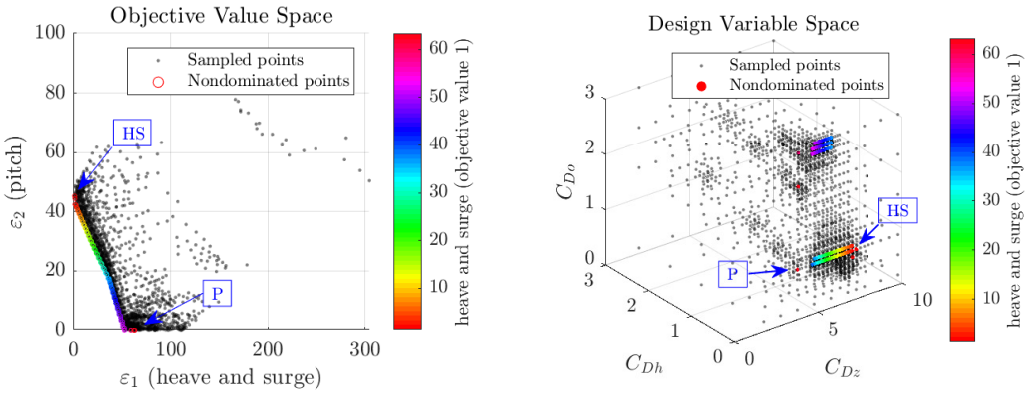

Figure 8. The Pareto front of the multiobjective formulation and the associated sampling points in the variable space, considering three variables

4. Discussion and Future Work

In this work, two different methods to calibrate viscous drag coefficients are applied: A manual decay test tuning and a new numerical optimization approach to calibrate drag coefficients for irregular waves. The calibration to the irregular sea state includes a single-objective optimization and a multiobjective optimization. Further, two different drag coefficient distributions are considered: One with a uniform transverse drag coefficient and an axial drag coefficient (referred to as 2 C_D) and one where the transverse drag coefficient is split into heave plate C_{Dh} and other

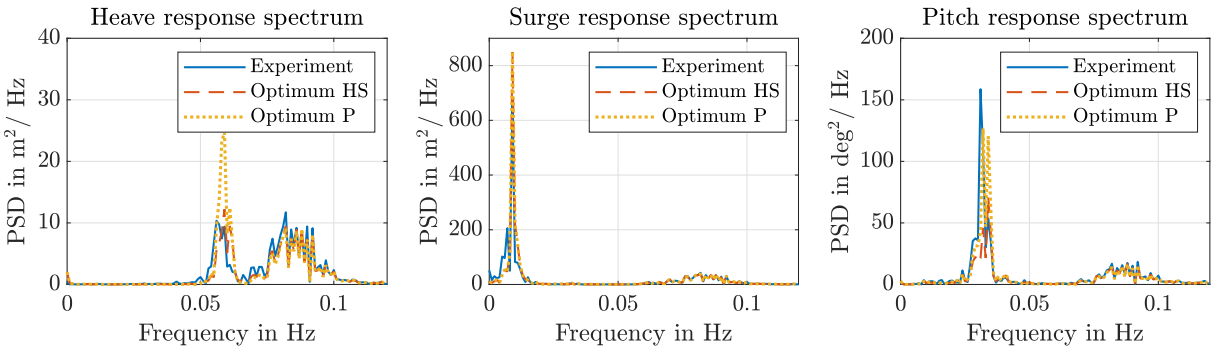

Figure 9. PSDs with optimized drag coefficients for heave, surge (HS) and pitch (P), using three design variables

components C_{Do}, resulting in three different C_D. The additional linear damping from the decay tests is adopted. All resulting drag coefficients are summarized in Figure 10. The differences between decay-test-tuned drag coefficients and those calibrated for an irregular sea state are significant. Regarding transverse drag coefficients, C_{Dh} from the decay test calibration is larger than C_{Do}. For the irregular wave, C_{Dh} is significantly smaller than C_{Do}. In pitch direction, optimal C_{Dz} for an irregular wave shows a deviation by a factor of 2. These findings highlight the necessity to improve the representation of drag, since the relevance of the choice of drag coefficients on the low-frequency wave forces has been shown in Tom et al. [16]. With this work, it was demonstrated that drag coefficients calibrated directly to the load case represent the irregular wave better than decay-test-tuned drag coefficients. Moreover, numerical optimization has proven to be a good method for calibration.

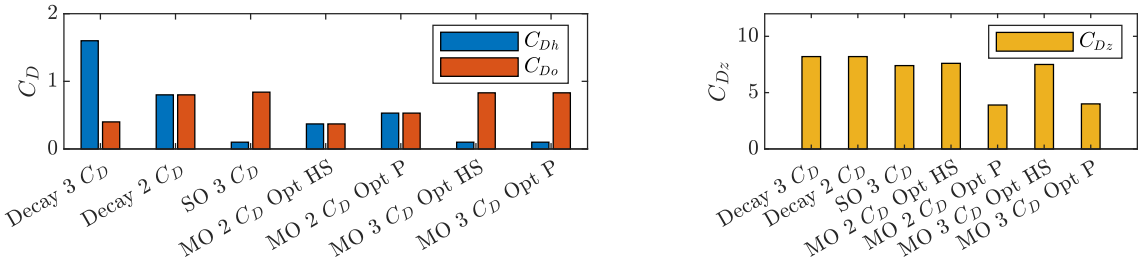

Figure 10. Comparison of resulting drag coefficients for decay tests, single-objective optimization (SO) and multiobjective optimization (MO) for irregular waves

For the decay tests, it was possible to calibrate the damping very well by fitting drag coefficients and adding a linear damping matrix. The physical source of the linear damping could not be determined, but has a similar magnitude compared to additional damping terms determined within the OC5 project [17]. This recurrence indicates that the linear damping is not due to a measurement error. Hence, this issue should be subject to prospective investigations, and further sources of damping should be evaluated. This evaluation should include external damping in the physical experiment and linear damping terms from the radiation computed with a potential flow solver.

During the optimization, noteworthy shortcomings in the hydrodynamic simulation were discovered, implying that further improvement of the hydrodynamic model is necessary. First of all, it is very peculiar that C_{Dh} converges to the lower boundary, as described in Sec. 3.3 and 3.5. Even though a smaller length-to-diameter ratio of the cylinder leads to smaller drag coefficients,

and drag has less influence on comparably large structures, a convergence toward zero is not expected and physically not reasonable. Considering the results found for both simulations with separate drag coefficients for heave plates, this indicates that a systematic error either in hydrodynamic modeling or in the experimental setup is present. The root cause for this error could not be determined conclusively.

Further, it became apparent that it is not possible to find an axial drag coefficient that simultaneously represents heave and pitch well. When applying an approach with only one velocity-independent axial drag coefficient, a trade-off needs to be accepted. This implies that an enhancement of the computation of drag should be considered. It is suspected that the simplifying assumption to apply the same set of drag coefficients for all load cases cannot be transferred to complex structures, which are floating and experience rotational motions. Additionally, neglecting the velocity dependence of the coefficient implied by the Reynolds number may also be an oversimplification for sophisticated floating structures. It might only be sufficiently accurate for cylindrical structures in fixed conditions like monopiles and jackets. Implementing velocity-dependent drag coefficients could lead to potential improvement, since the difference between drag coefficients for a cylinder under laminar flow at low Reynolds numbers and under turbulent flow under high Reynolds numbers is significant. In an irregular sea state, the velocity varies and flow can stagnate. Hence, it is conceivable to implement a routine that adjusts the drag coefficients according to the Reynolds number. Additionally, the incorporation of an axial drag coefficient that depends on the angle by which the structure is tilted could be considered. Further, when transferring drag coefficients from the 1/50 scale model experiment to the full scale, it has to be considered that the Reynolds number is not preserved. This discrepancy should be compensated when the model-scale experimental results are applied to the full-scale OpenFAST model.

Acknowledgements

This work is based on the Masters Thesis of M. Böhm. The supervision of A. Robertson and C. Hübler is highly appreciated and the research stay was facilitated by the partial scholarship "Leibniz PROMOS" of the International Office, Leibniz Universität Hannover. This work was authored [in part] by the National Renewable Energy Laboratory, operated by Alliance for Sustainable Energy, LLC, for the U.S. Department of Energy (DOE) under Contract No. DE-AC36-08GO28308. Funding provided by the U.S. Department of Energy Office of Energy Efficiency and Renewable Energy Wind Energy Technologies Office. The views expressed in the article do not necessarily represent the views of the DOE or the U.S. Government. The U.S. Government retains and the publisher, by accepting the article for publication, acknowledges that the U.S. Government retains a nonexclusive, paid-up, irrevocable, worldwide license to publish or reproduce the published form of this work, or allow others to do so, for U.S. Government purposes. Further, we gratefully acknowledge the financial support of the Deutsche Forschungsgemeinschaft (DFG, German Research Foundation) for the ENERGIZE project (436547100).

References

[1] Eurostat. 30% of electricity generated from renewable sources `https://ec.europa.eu/eurostat/web/products-eurostat-news/-/DDN-20180921-1`, accessed: December 2019.
[2] WindEurope 2017. Floating offshore wind vision statement. *WindEurope Report.*
[3] James R and Ros MC 2015. Floating Offshore Wind: Market and Technology Review.
[4] Robertson A et al 2017. OC5 Project Phase II: Validation of Global Loads of the DeepCwind Floating Semisubmersible Wind Turbine. *Energy Procedia* **137** 38-57.
[5] Wendt F, Robertson A and Jason J 2017. FAST Model Calibration and Validation of the OC5-DeepCwind Floating Offshore Wind System Against Wave Tank Test Data. *ISOPE 2017 27th International Ocean and Polar Engineering Conference.*

[6] Berthelsen PA, Bachynski EE, Karimirad M and Thys M 2016. Real-Time Hybrid Model tests of a braceless semi-submersible wind turbine: Part III calibration of a numerical model. *ASME 2016 35th International Conference on Ocean, Offshore and Arctic Engineering.*
[7] Kvittem MI, Berthelsen PA, Eliassen L and Thys M 2018. Calibration of Hydrodynamic Coefficients for a Semi-Submersible 10 MW Wind Turbine. *ASME 2018 37th International Conference on Ocean, Offshore and Arctic Engineering.*
[8] Lemmer F, Yu W, Cheng PW, Pegalajar-Jurado A, Borg M, Mikkelsen RF and Bredmose H 2018. The TripleSpar Campaign: Validation of a Reduced-Order Simulation Model for Floating Wind Turbines. *ASME 2018 37th International Conference on Ocean, Offshore and Arctic Engineering.*
[9] Robertson A, Bachynski E, Gueydon S, Wendt F and Schünemann P 2020.Total experimental uncertainty in hydrodynamic testing of a semisubmersible wind turbine, considering numerical propagation of systematic uncertainty. *Ocean Engineering* **195** 106605.
[10] OpenFAST `https://github.com/OpenFAST/openfast`, accessed: December 2019.
[11] Robertson A, Bachynski E, Gueydon S, Wendt F, Schünemann P and Jonkman J 2018. Assessment of Experimental Uncertainty for a Floating Wind Semisubmersible Under Hydrodynamic Loading. *ASME 2018 37th International Conference on Ocean, Offshore and Arctic Engineering.*
[12] Helder J and Pietersma M 2013. UMaine- DeepCwind/OC4 Semi Floating Wind Turbine Repeat Tests. MARIN Report No. 27005-1-OB.
[13] Haid L, Stewart G, Jonkman J, Robertson A, Lackner M and Matha D 2013. Simulation length requirements in the loads analysis of offshore floating wind turbines. *ASME 2013 32th International Conference on Ocean, Offshore and Arctic Engineering.*
[14] Hofmeister B, Bruns M and Rolfes R 2019. Finite element model updating using deterministic optimisation: A global pattern search approach. *Engineering Structure* **195** 373-381.
[15] Goldberg DE 1989. *Genetic Algorithms in Search, Optimization and Machine Learning* (Boston, USA: Addison-Wesley Longman Publishing Co., Inc.).
[16] Tom N, Robertson A, Jonkman J, Wendt F and Böhm M 2019. Bichromatic Wave Selection for Validation of the Difference-Frequency Transfer Function for the OC6 Validation Campaign. *ASME 2019 2nd International Offshore Wind Technical Conference.*
[17] Wendt F, Andersen MT, Robertson A, and Jonkman J 2016. Verification and Validation of the New Dynamic Mooring Modules Available in FAST v8. *ISOPE 2016 26th International Ocean and Polar Engineering Conference.*